RSC Advances

PAPER

View Article Online
View Journal | View Issue

Open Access Article. Published on 19 May 2020. Downloaded on 2/10/2026 4:56:31 PM.
This article is licensed under a Creative Commons Attribution-NonCommercial 3.0 Unported Licence.

Check for updates

Cite this: *RSC Adv.*, 2020, **10**, 19020

Novel hypophosphite hybrid perovskites of $[CH_3NH_2NH_2][Mn(H_2POO)_3]$ and $[CH_3NH_2NH_2][Mn(H_2POO)_{2.83}(HCOO)_{0.17}]$ exhibiting antiferromagnetic order and red photoluminescence†

Mirosław Mączka,* Anna Gągor, Adam Pikul and Dagmara Stefańska

Hybrid perovskites based on hypophosphite ligands constitute an emerging family of compounds exhibiting unusual structures and offering a platform for construction of novel functional materials. We report the synthesis, crystal structure, and magnetic and optical properties of novel undoped and $HCOO^-$-doped manganese hypophosphite frameworks templated by methylhydrazinium cations. The undoped compound crystallizes in a three-dimensional perovskite-like orthorhombic structure, space group *Pnma*, with ordered organic cations located in windows between the perovskite cages expanding along the *a*-direction. Both conventional anti-phase tilting, unconventional in-phase tilting and columnar shifts in the *a*-direction are present. Doping with $HCOO^-$ ions has a insignificant influence on the crystal structure but leads to a decrease of the unit cell volume. Magnetic studies indicate that these compounds order antiferromagnetically at $T_N = 6.5$ K. Optical studies indicate that they exhibit red photoluminescence under 266 nm excitation with the activation energy for thermal quenching of 98 and 65 meV for the undoped and doped sample, respectively. For the undoped sample, the emission lifetime reaches 5.05 ms at 77 K but it decreases to 62.26 μs at 300 K. The low value of the activation energy and huge temperature dependence of photoluminescence intensity suggest a high potential of these hypophosphites for non-contact temperature sensing.

Received 16th April 2020
Accepted 12th May 2020

DOI: 10.1039/d0ra03397a

rsc.li/rsc-advances

Introduction

Hybrid organic–inorganic compounds have been the subject of intense studies because their diverse structural and chemical variability offers unlimited opportunities for tuning their physical and chemical properties by chemical modification of the organic and/or inorganic part. One of the most important sub-groups of such hybrid compounds is halides, which have attracted a lot of attention in recent years due to their excellent optoelectronic properties.[1–11] In particular, they are promising materials for applications in solar cells, which were shown to demonstrate power conversion efficiency of over 22%.[1,6–9] They are also attractive materials exhibiting one-photon[2–5,10] and multiphoton-excited upconversion photoluminescence.[4,11]

Another interesting class of compounds are molecular perovskites built of $M^{II}O_6$ and $M^{II}N_6$ octahedra (M^{II} = Cd, Mg, Zn, Mn, Co, Fe, Cu, Ni) connected by short organic linkers such as formate ($HCOO^-$), azide (N_3^-), cyanide (CN^-), dicyanamide ($N(CN)_2^-$, *dca*$^-$) and hypophosphite ($H_2PO_2^-$), which possess large cavities occupied by organic cations.[12–28] In this family of compounds, formates attracted a lot of attention due to their multiferroic properties[14–16] while azides, dicyanamides and cyanides showed switchable dielectric behaviour, ferroelectric, luminescent, ferroelastic and non-linear optical properties.[15–25] Dicyanamide-linked polymers were also shown to be promising barocaloric materials.[26–28]

In contrast to widely studied formates, azides, dicyanamides and cyanides, family of hybrid perovskites based on hypophosphite ligand was discovered quite recently, in year 2017, and only six such compounds are known.[29–32] The reported data show that this new emerging family of perovskites based on hypophosphite anion may show even more interesting physicochemical properties than formates, azides or dicyanamides. For instance, it was shown that whereas dimethylammonium (DMA^+) cation is located in the center of the perovskite cage in multiferroic $[DMA][Mn(HCOO)_3]$, in the hypophosphite analogue this cation sits inside the windows between perovskite

Institute of Low Temperature and Structure Research, Polish Academy of Sciences, Box 1410, 50-950 Wrocław 2, Poland. E-mail: m.maczka@int.pan.wroc.pl

† Electronic supplementary information (ESI) available: Tables S1 and S2: crystallographic data. Fig. S1–S9: XRD patterns, the position of organic cations in the structure, absorption spectra, temperature-dependent photoluminescence, colour coordinate and emission decay curves for $HCOO^-$-doped compound, schematic illustration of luminescence mechanism. CCDC 1989064–1989066. For ESI and crystallographic data in CIF or other electronic format see DOI: 10.1039/d0ra03397a

This journal is © The Royal Society of Chemistry 2020

Open Access Article. Published on 19 May 2020. Downloaded on 2/10/2026 4:56:31 PM.
This article is licensed under a Creative Commons Attribution-NonCommercial 3.0 Unported Licence.

cages.[30] This unusual behavior is related to different hydrogen bond network in formate and hypophosphite analogues, *i.e.*, hydrogen bonds drive the structural distortion and off-centering in the hypophosphite.[30] Furthermore, the known hypophosphites showed presence of unconventional tilts and columnar shifts.[30,33] Thus, it has been argued that hypophosphites have higher than formates potential for symmetry breaking and this feature could lead to improper ferroelectricity or other functional properties.[30] It is worth to add here that although magnetic data were reported only for two representatives, formamidinium (FA) and guanidinium (GUA) manganese hypophosphites, discovery of long-range magnetic order with a Néel temperature of 6.5 K for the latter compound[29] proves that hypophosphite-based perovskites might also show interesting magnetic properties.

Since perovskite-like hypophosphites may exhibit various physicochemical properties, we have decided to search for novel perovskites constructed with H_2POO^- ligand. Herein, we show that a new hypophosphite can be synthesized using methylhydrazinium (MHy^+) cations. We report studies of its structure as well as magnetic, optical and luminescent properties.

Experimental details

Materials and instrumentation

Manganese (II) carbonate (99.9%, Sigma-Aldrich), hypophosphorous acid (50% w/w aqueous solution, Supelco), methylhydrazine (98%, Sigma-Aldrich) and formic acid (98%, Sigma-Aldrich) were commercially available and used without further purification. Elemental analysis (C, H, N) was performed on a Elementar CHN/O FlashSmart analyzer. Powder X-ray diffraction was collected on X'Pert PRO powder diffractometer operating with Cu Kα radiation. Magnetization of a large number of freely oriented single crystals of $[MHy][Mn(H_2POO)_3]$ (about 120 mg in total) and $[MHy][Mn(H_2POO)_{2.83}(HCOO)_{0.17}]$ (90 mg) was measured using a commercial SQUID magnetometer in the temperature range 1.7–300 K and in external magnetic fields up to 50 kOe. The background coming from a weakly diamagnetic sample holder was found to be negligible in comparison to the total signal, hence its subtraction was omitted. For measurements of the absorption spectra, the Varian Cary 5E UV-Vis-NIR spectrophotometer was used. Temperature-dependent emission spectra under 266 nm excitation from a diode laser (10 mW power) were measured with the Hamamatsu photonic multichannel analyzer PMA-12 equipped with a BT-CCD linear image sensor. The temperature was controlled applying Linkam THMS 600 Heating/Freezing Stage. Decay profiles were recorded with a Lecroy digital oscilloscope and the Nd:YAG laser as an excitation source.

Synthesis

In order to grow single crystals of $[MHy][Mn(H_2POO)_3]$, manganese carbonate (0.575 g, 5 mmol) was dissolved in hypophosphorous acid (6.46 mL, 60 mmol). The solution was heated to 50 °C and stirred. Then 10 mmol of methylhydrazine (0.5 mL) was added and the mixture was left at 50 °C in air. Faint pink crystals that grew overnight were separated from the mother liquid, washed with methanol and dried at room temperature. Anal. Calcd for $[MHy][Mn(H_2POO)_3]$ (%): C, 4.03; H, 4.42; N, 9.29; found (%): C, 4.04; H, 4.38; N, 9.43. Comparison of the powder XRD pattern with the calculated one based on the single-crystal data attests phase purity of powdered sample (Fig. S1 in the ESI†).

We also tried to obtain mixed formate–hypophosphite crystals using the same procedure and 1 : 1 molar ratio of hypophosphorous and formic acid. Unfortunately, the obtained crystals contained small amount of $HCOO^-$. Chemical composition found for $[MHy][Mn(H_2POO)_{3-x}(HCOO)_x]$ (%): C, 4.77; H, 4.43; N, 9.51. From C/N ratio, $x = 0.17$.

Single-crystal X-ray diffraction

The single-crystal X-ray diffraction was performed for pure $[MHy][Mn(H_2POO)_3]$ at room temperature (RT) and 100 K, and for formate doped crystals of $[MHy][Mn(H_2POO)_{2.83}(HCOO)_{0.17}]$ formula at RT. The four-circle Xcalibur diffractometer operating with Mo Kα radiation source and CCD Atlas detector was used for data collection. Absorption was corrected by multi-scan methods in CrysAlis PRO 1.171.38.43 (Rigaku Oxford Diffraction, 2015). The details of the crystals, data collections and refinements are given in Table S1.† The low-temperature refinement confirmed the stability of the orthorhombic *Pnma* symmetry down to 100 K. Table S2† shows selected geometrical parameters. For all structures, H-atoms were introduced at calculated positions and refined with constrained parameters. In the formate doped crystals the dopant amount was constrained to the value obtained from the elemental analysis. However, free refinement gave very similar results. Formate groups were localized only in one of two symmetry allowed sites, at the position of hypophosphite ligand linking two Mn^{2+} centers in the evident *anti–anti* bonding.

Results and discussion

Single-crystal X-ray diffraction

$[MHy][Mn(H_2POO)_3]$ crystallizes in the orthorhombic system, in the *Pnma* space group. The inorganic part of the structure comprises one symmetry independent metal center and two distinct hypophosphite ligands, one H_2POO^- unit of C_1 symmetry that connects neighbouring Mn^{2+} ions in (101) planes through *anti–anti* bonding, with two P–O–Mn angles of 127° and 130°, and one-half of another hypophosphite group of C_s symmetry that acts as a linker along [010] direction with P–O–Mn angles around 157°. This flexible binding capability in conjunction with the H-bonding-driven off-centering of cations leads to a considerably different structure compared to the formate analogue. In $[MHy][Mn(HCOO)_3]$ the planar *anti–anti* connection modes in combination with the narrow range of binding angles, which is characteristic to formates, prevent large framework distortions and cations displacements from the centers of perovskite cages, where they perform thermally induced rotations.[14] The adjustable hypophosphite framework

Open Access Article. Published on 19 May 2020. Downloaded on 2/10/2026 4:56:31 PM.
This article is licensed under a Creative Commons Attribution-NonCommercial 3.0 Unported Licence.

in [MHy][Mn(H_2POO)$_3$] accommodates notable off-center shifts of MHy^+ (Fig. 1a and b). The high obtuse P–O–Mn angle opens the window between the perovskite cages and allows for location of MHy^+ inside these windows expanding along the *a*-direction. The off-center placement of amines is driven by the N–H···OH-bonding and results in the lower symmetry of hypophosphite framework (*Pnma*) compared to the formate (*R*3*c* at RT). Similar, strongly off-centered distribution of protonated amines and lowering of symmetry was encountered in [DMA][Mn(H_2POO)$_3$] and [GUA][Mn(H_2POO)$_3$].[29,30] Opposite to formate analogue, MHy^+ cations are ordered at RT and interact with hypophosphite oxygen atoms *via* hydrogen bond interactions of medium strength (Fig. 1c and d). It is worth noting that both amine groups are involved in H-bonds, opposite to the formate analogue, where only the middle NH_2 groups may interact with the framework at RT. As a result, the H-bonds in the hypophosphite are strong enough to overcome thermally induced rotational motions of MHy^+ and these cations are ordered. The hydrogen bonds parameters are given in Table 1. Fig. S2† shows the placement of MHy^+ cations in the structure in the space feeling model.

The inorganic substructure yields R_5^- distortion mode and propagation vector $\mathbf{k} = [\frac{1}{2}, \frac{1}{2}, \frac{1}{2}]$. Fig. 2 shows tilt and shift matrixes together with the structure viewed along the normal to the three pseudo-perovskite cubic axes. The conventional *anti-phase* tilting is present down the cubic *a*- and *b*-direction and in all (100), (010), (001) planes. Toward the *b*-direction, the structure accommodates unconventional *in-phase* tilting. The shift matrix is similar to that found in [GUA][Mn(H_2POO)$_3$]. There are active shifts in the *a*-direction with in-phase correlation in the *c*-direction.

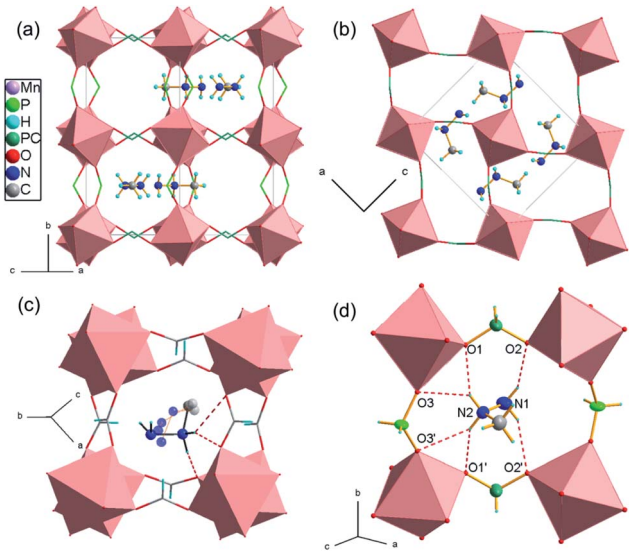

Fig. 1 (a and b) the crystal structure packing of [MHy][Mn(H_2POO)$_3$] toward two pseudo-cubic directions, (c) the distorted perovskite structure of [MHy][Mn(HCOO)$_3$] with a disordered MHy^+, (d) the hydrogen bonds anchoring the MHy^+ within Mn–hypophosphite framework. The dark green stands for the mixed P/C sites in the doped compound.

Table 1 Selected hydrogen-bond parameters[a]

D–H···A	D–H (Å)	H···A (Å)	D···A (Å)	D–H···A (°)
I				
N2–HB···O1^{i}	0.89	2.08	2.875 (2)	148.4
N2–HB···O3^{ii}	0.89	2.53	3.176 (5)	130.5
N2–HC···O1	0.89	2.08	2.875 (2)	148.4
N2–HC···O3^{iii}	0.89	2.53	3.176 (5)	130.5
N1–HA···O2^{i}	0.87	2.24	3.001 (3)	146.8
II				
N2–HB···O1^{i}	0.89	2.05	2.8461 (18)	147.7
N2–HB···O3^{ii}	0.89	2.48	3.122 (3)	129.6
N2–HC···O1	0.89	2.05	2.8461 (18)	147.7
N2–HC···O3^{iii}	0.89	2.48	3.122 (3)	129.6
N1–HA···O2^{i}	0.86	2.20	2.977 (2)	150.9
III				
N2–HB···O1^{i}	0.89	2.08	2.871 (2)	148.0
N2–HB···O3^{ii}	0.89	2.51	3.164 (4)	130.6
N2–HC···O1	0.89	2.08	2.871 (2)	148.0
N2–HC···O3^{iii}	0.89	2.51	3.164 (4)	130.6
N1–HA···O2^{i}	0.87	2.21	2.994 (2)	150.1

[a] Symmetry code(s): (i) $x, -y + 1/2, z$; (ii) $-x + 1/2, y - 1/2, z + 1/2$; (iii) $-x + 1/2, -y + 1, z + 1/2$.

In the formate doped [MHy][Mn(H_2POO)$_3$], the formate groups seem to locate exclusively in the position of C_1 symmetry that links two Mn^{2+} centres *via* pronounced *anti–anti* coordination mode with two P–O–Mn angles of 128° and 130°. Such a preference is in line with the fact that formates strongly prefer *anti–anti* bonding in the perovskite topology.[33] The relatively low concentration of $HCOO^-$ groups has insignificant influence on the crystal structure; however, it slightly disturbs the crystal volume that decreases from 1078 Å^3 in pure hypophosphite to 1071 Å^3 in doped one.

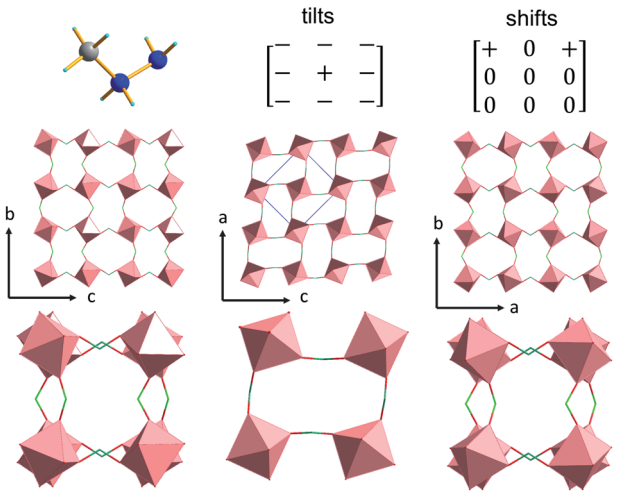

Fig. 2 Tilts and shifts of orthorhombic [MHy][Mn(H_2POO)$_3$]. The axes show pseudo-cubic directions; (above) MHy^+ with tilt and shift matrixes; (below) single 4 × 4 octahedral layers and stacked 2 × 2 layers.

Open Access Article. Published on 19 May 2020. Downloaded on 2/10/2026 4:56:31 PM.
This article is licensed under a Creative Commons Attribution-NonCommercial 3.0 Unported Licence.

Magnetic studies

As can be inferred from Fig. 3a, [MHy][Mn(H_2POO)$_{2.83}$(HCOO)$_{0.17}$] exhibits at elevated temperatures paramagnetic behavior with linear T-dependence of χ^{-1} above about 10 K. The experimental curve can be described in this temperature range by the conventional Curie–Weiss law $\chi(T) = C(T - \theta_p)$, where C is the Curie constant and θ_p is the paramagnetic Curie–Weiss temperature. Least-squares fitting procedure yielded the values $C = 3.89(1)$ emu mol^{-1} K and $\theta_p = -9.4(1)$ K (see the thick solid line in Fig. 3a, left axis).

The effective magnetic moment μ_{eff} derived from the Curie constant as $\mu_{eff} = \sqrt{8C}$ is equal to 5.58(1) μ_B. This value is lower than (but still close to) the theoretical value calculated for Mn^{2+} ions with the electron configuration $3d^5$: the effective magnetic moment calculated for such a configuration within the Russel–Saunders coupling scheme ($S = 5/2$, $L = 0$, $J = 5/2$ and $g_J = 2$) is equal to $\mu_{Mn^{2+}} = g_J\sqrt{S(S+1)}\mu_B = 5.92\mu_B$ (for details see *e.g.* ref. 34).

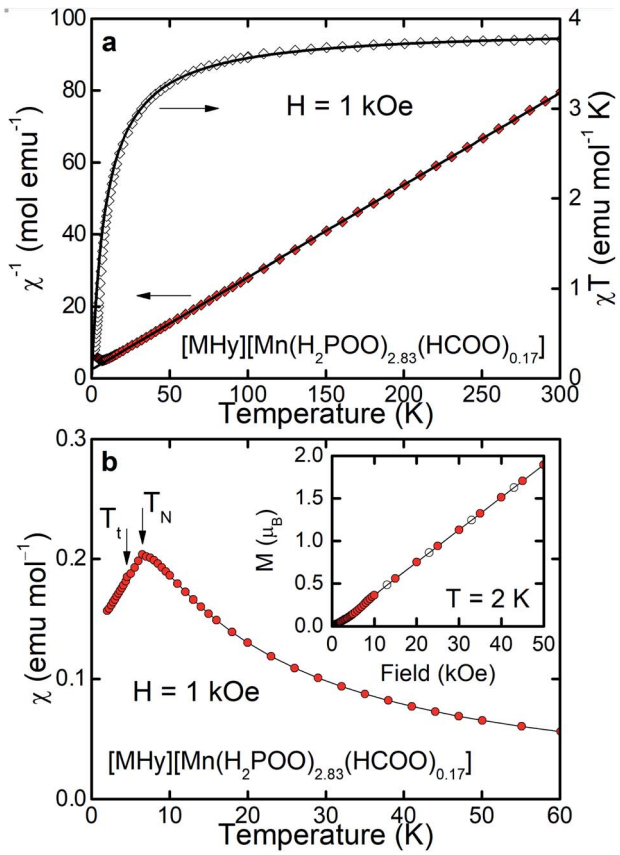

Fig. 3 (a) Inverse magnetic susceptibility χ^{-1} and product χT of [MHy][Mn(H_2POO)$_{2.83}$(HCOO)$_{0.17}$] (left and right axis, respectively) measured as a function of temperature in steady external magnetic field H. Thick solid curves are a fit of the Curie–Weiss law to the experimental data (for details see the text). (b) Temperature dependence of χ of the compound. Inset: magnetization M *vs.* H measured with increasing and decreasing field (open and closed symbols, respectively). T_N and T_t mark phase transition temperatures and thin solid lines serve as a guide for the eye.

The negative value of θ_p indicates presence of predominant antiferromagnetic coupling between the magnetic moments of Mn^{2+}, which can be inferred also from the overall behavior of the product χT (Fig. 3a, right axis). In particular, at RT χT achieves a value of about 3.8 emu mol^{-1} K, which is close to the experimental value of the Curie constant (*i.e.* 3.89 emu mol^{-1} K) and noticeably lower that the theoretical value of the Curie constant expected for non-interacting Mn^{2+} ions, *i.e.* $C = \frac{1}{8}\mu_{Mn^{2+}}{}^2 = \frac{1}{8}5.92^2 = 4.38$ emu mol^{-1} K. As a consequence of the postulated antiferromagnetic coupling, the $\chi T(T)$ curve bends towards lower values upon decreasing temperature.

As can be inferred from Fig. 3b, the compound orders antiferromagnetically at $T_N = 6.5$ K, absolute value of which is of the same order of magnitude as θ_p derived from the Curie–Weiss fit. Linear field dependence of the magnetization $M(H)$ of [MHy][Mn(H_2POO)$_{2.83}$(HCOO)$_{0.17}$] (see the inset to Fig. 3b) and lack of any hysteresis in $M(H)$ confirm the latter hypothesis. At the highest field applied M achieves a value of 1.89 μ_B, which is far from the saturated magnetic moment expected for Mn^{2+}, *i.e.* $\mu_{sat} = g_J = 5$ μ_B, corroborating once more the antiferromagnetic character of the ordering.

It must be noted, however, that in the magnetically ordered range another anomaly in $\chi(T)$ is hardly visible at $T_t = 4.5$ K, which can be associated with a tiny deviation of $M(H)$ from linearity at about 5–10 kOe. We suppose that this anomaly manifests presumably some small rearrangement of antiferromagnetically ordered moment of Mn^{2+} ions, but making final conclusion is of course difficult without more sophisticated experiments.

Results of magnetization measurements carried out for [MHy][Mn(H_2POO)$_3$] are gathered in Fig. 4. As can be seen, its magnetic properties are very similar to those observed for the $HCOO^-$-doped compound. In particular, the Curie–Weiss fit performed for [MHy][Mn(H_2POO)$_3$] (see the solid lines in Fig. 4a) yielded the parameters: $C = 4.08(1)$ emu mol^{-1} K and $\theta_p = -9.3(1)$ K (see the thick solid line in Fig. 4a, left axis) – very close to those obtained for [MHy][Mn(H_2POO)$_{2.83}$(HCOO)$_{0.17}$]. The effective magnetic moment derived from C is of about 5.71 μ_B, which is even closer to the theoretical one (5.92 μ_B). The RT value of χT (*i.e.* 3.95 emu mol^{-1} K) is close to the experimental value of the Curie constant (4.08 emu mol^{-1} K) and the $\chi T(T)$ curve bends towards lower values upon cooling down the sample. The long-range antiferromagnetic order occurs in the [MHy][Mn(H_2POO)$_3$] compound at the Néel temperature of 6.5 K and is followed by a tiny anomaly at $T_t = 4.5$ K (see the inset to Fig. 4b), being exactly the same as in [MHy][Mn(H_2POO)$_{2.83}$(HCOO)$_{0.17}$]. The antiferromagnetic order of [MHy][Mn(H_2POO)$_3$] is confirmed by linear variation of $M(H)$ (see the inset to Fig. 4b) with hardly visible deviation at about 5–10 kOe, presumably associated with the spin-rearrangement detected at T_t. It is worth adding that the same Néel temperature and very similar Weiss constant of −9.3(1) K were previously reported also [GUA][Mn(H_2POO)$_3$] whereas [FA][Mn(H_2POO)$_3$] do not order magnetically down to 2 K.[29] It should also be noticed that the formate analogue, [MHy][Mn(HCOO)$_3$], also exhibits antiferromagnetic order but with slightly larger $T_N = 9.0$ K.[14] This behavior is consistent with stronger superexchange interactions

Open Access Article. Published on 19 May 2020. Downloaded on 2/10/2026 4:56:31 PM.
This article is licensed under a Creative Commons Attribution-NonCommercial 3.0 Unported Licence.

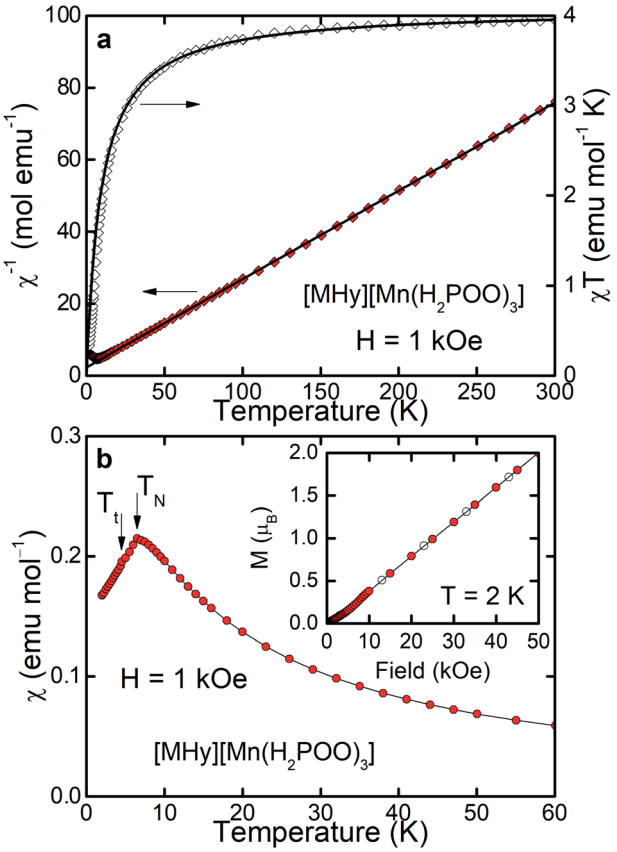

Fig. 4 Magnetic properties of [MHy][Mn(H$_2$POO)$_3$] measured and displayed in the same way as properties of [MHy][Mn(H$_2$POO)$_{2.83}$(HCOO)$_{0.17}$] shown in Fig. 3., *i.e.*, panel (a) shows inverse magnetic susceptibility χ^{-1} and product χT whereas panel (b) illustrates temperature dependence of χ.

in the formate compared to hypophosphite due to shorter Mn⋯Mn distances in [MHy][Mn(HCOO)$_3$] (6.0297–6.1187 Å at 100 K)[14] compared to [MHy][Mn(H$_2$POO)$_3$] (6.277 and 6.6302 Å at 100 K).

The observed similarity of the magnetic properties of the systems studied is not a big surprise. Although the crystal structures of the parent systems [MHy][Mn(H$_2$POO)$_3$] and [MHy][Mn(HCOO)$_3$] are considerably different, the concentration of the HCOO groups in [MHy][Mn(H$_2$POO)$_{2.83}$(HCOO)$_{0.17}$] is very small, leading to very small modification of the crystal structure. Therefore, one can expect that the leading factors governing the magnetic ground state of [MHy][Mn(H$_2$POO)$_{2.83}$(HCOO)$_{0.17}$], *i.e.* the oxidation state (and hence the electron configuration) of the manganese ions, their environment (local symmetry and ligands), and the exchange interactions between Mn^{2+} (depending on i.a. Mn–Mn distances and P–O–Mn angles), remain nearly the same as in [MHy][Mn(H$_2$POO)$_3$].

Optical studies

Diffuse reflectance spectra of the studied samples are shown in Fig. S3 and S4.† The spectra consist of an intense band centered at 220 nm (45 455 cm^{-1}) associated with matrix absorption. Above 250 nm the broad tail ascribed to overlapped O^{2-}–Mn^{2+} charge transfer (CT) band with the host absorption band was detected. Moreover, a few peaks with smaller intensity are observed in the 300–550 nm range that are characteristic for Mn^{2+} ions in octahedral coordination (Fig. S3 and S4†). These bands are more clearly observed for [MHy][Mn(H$_2$POO)$_{2.83}$(HCOO)$_{0.17}$] and they can be attributed to the electron transitions from $^6A_{1g}$(S) ground level to $^4T_{1g}$(P) (312 nm), ^4E(D) (339 nm), $^4T_{2g}$(D) (357 nm), $^4A_{1g}$ (401 nm), ^4E_g(G) (404 nm), $^4T_{2g}$(G) (440 nm) and $^4T_{1g}$(G) (527 nm) excited states.[35–37]

Using the RT diffuse reflectance spectra, we determined the energy bandgap (E_g) of investigated hypophosphites with the Kubelka–Munk relation:[38]

$$F(R) = \frac{(1-R)^2}{2R}$$

were R denotes reflectance. Fig. S5 and S6† show that the energy bandgap of the [MHy][Mn(H$_2$POO)$_3$] and [MHy][Mn(H$_2$POO)$_{2.83}$(HCOO)$_{0.17}$] samples is 5.32 and 5.34 eV, respectively. These values are larger than reported values for Mn-based dicyanamides (4.95–5.17 eV).[28,37]

[MHy][Mn(H$_2$POO)$_3$] exhibits red emission at 80 K with maximum at 686 nm (14 577 cm^{-1}, CIE chromacity (0.7, 0.3)) (Fig. 5a and b) that can be attributed to the $^4T_{1g}$(G) → $^6A_{1g}$(S) transition of Mn^{2+} ions. This emission is red-shifted compared to Mn-based dicyanamides (maximum near 630 nm) and perovskite-type pyrrolidinium manganese halides with octahedral coordination of Mn^{2+} ions (maximum near 615–645 nm).[28,37,39] Since the energy of the $^4T_{1g}$(G) → $^6A_{1g}$(S) transition decreases with increasing crystal field strength,[40] the observed red shift of the emission points to higher crystal field strength in the studied hypophosphites.

The Mn^{2+} emission quenches very quickly (Fig. 5c), much faster than emission of tetrapropylammonium manganese and tributylammonium manganese discyanamides.[28,37] Such pronounced temperature dependence of emission intensity

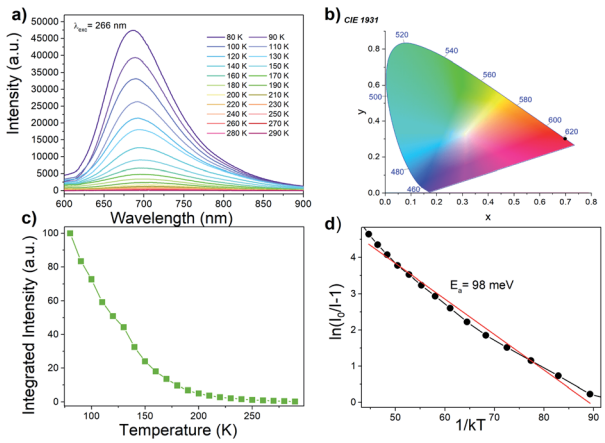

Fig. 5 (a) The temperature dependent emission spectra of [MHy][Mn(H$_2$POO)$_3$] excited at 266 nm, (b) CIE coordinate at 80 K (black dot), (c) integrated emission intensity as a function of temperature and (d) a activation energy of the thermal quenching.

Open Access Article. Published on 19 May 2020. Downloaded on 2/10/2026 4:56:31 PM.
This article is licensed under a Creative Commons Attribution-NonCommercial 3.0 Unported Licence.

suggests that [MHy][Mn(H_2POO)$_3$] has high potential for noncontact temperature sensing. The energy activation for thermal quenching, E_a, was calculated using Arrhenius formula:[41]

$$I(T) = \frac{I_0}{1 + e^{-E_a/k_B T}}$$

where I is the intensity at a given temperature, I_0 is the initial intensity of emission, c is a constant for a certain host and k is the Boltzmann constant. Linear fitting of $\ln(I_0/I - 1)$ *vs.* $1/kT$ shows that the activation energy for thermal quenching is about 98 meV (Fig. 5d).

Luminescence decay can be can be best fitted by bi-exponential decay function with $\tau_1 = 243$ μs and $\tau_2 = 5.05$ ms at 77 K (Fig. 6a). The shorter life time can be most likely attributed to nonradiative processes. The emission lifetime strongly decreases with increasing temperature and at 300 K equals to $\tau_1 = 11.13$ μs and $\tau_2 = 62.26$ μs (Fig. 6b). The significant shortening of the decay time with temperature indicates that nonradiative processes play an important role in the investigated hypophosphite.[42] It is worth adding that significantly shorter lifetime was reported for tetrapropylammonium manganese dicyanamide (5.88 μs at 300 K), for which the luminescence decay was monoexponential.[37]

Very similar emission is also observed for [MHy][Mn(H_2POO)$_{2.83}$($HCOO$)$_{0.17}$] (Fig. S7†). However, doping with $HCOO^-$ ions leads to decrease of the activation energy for thermal quenching to 65 meV (Fig. S7d†). Furthermore, the lifetime of the emission measured at 77 K is approximately two times shorter compared to the undoped sample (Fig. S8†).

A possible mechanism of Mn^{2+} luminescence in the investigated samples is presented in Fig. S9.† Excitation at UV region (266 nm) leads to transfer of the electron to the O^{2-}–Mn^{2+} CT band. Subsequently, nonradiative depopulation of the CT band leads to the population of the $^4T_1$(G) excited state of Mn^{2+}. Similar excitation path was recently reported by Lin *et. al.*[43] With the increasing temperature, the $^4T_1$(G) excited state of Mn^{2+} is depopulated due to the intercrossing of its parabola with the parabola of $^6A_{1g}$(S) ground state. This process is thermally dependent with the activation energy of 98 and 65 meV for [MHy][Mn(H_2POO)$_3$] and [MHy][Mn(H_2POO)$_{2.83}$($HCOO$)$_{0.17}$], respectively.

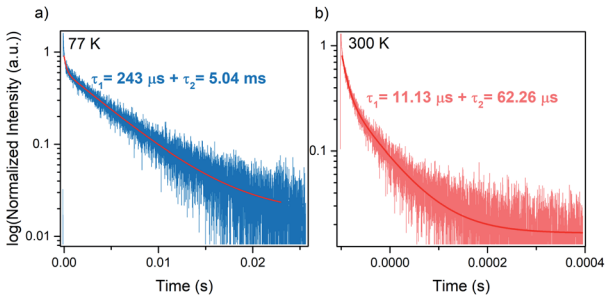

Fig. 6 Emission decay curves of [MHy][Mn(H_2POO)$_3$] at (a) 77 K and (b) 300 K.

Conclusions

We report that MHy^+ cations can be used for construction of a new manganese hypophosphite perovskite-like framework. [MHy][Mn(H_2POO)$_3$] crystallizes in the orthorhombic system, in the *Pnma* space group. This is the highest symmetry reported up to now for any hypophosphite framework templated by monovalent cations. The characteristic feature of the crystal structure is strongly off-centered distribution of MHy^+ cations. Studies of magnetic properties reveal that this compound orders antiferromagnetically at 6.5 K. Thus, [MHy][Mn(H_2POO)$_3$] is the second perovskite-type hypophosphite exhibiting magnetic order.

We also report studies of optical properties of [MHy][Mn(H_2POO)$_3$] and [MHy][Mn(H_2POO)$_{2.83}$($HCOO$)$_{0.17}$] samples. To the best of our knowledge, this is the first report on such studies for of any hypophosphite. These studies show that both samples exhibit red emission at 77 K with the energy activation for thermal quenching of 98 and 65 meV for undoped and $HCOO^-$-doped sample, respectively. The emission decay time at 77 K is of ms order and it decreases for the doped sample, indicating enhancement of nonradiative processes on $HCOO^-$ doping. Interestingly, in contrast to manganese dicyanamide frameworks, exhibiting relatively weak temperature dependence of the emission intensity, the Mn^{2+} emission of [MHy][Mn(H_2POO)$_3$] and [MHy][Mn(H_2POO)$_{2.83}$($HCOO$)$_{0.17}$] quenches very quickly suggesting a high potential of these hypophosphites for non-contact temperature sensing.

Conflicts of interest

There are no conflicts of interest to declare

Acknowledgements

This research was supported by the National Science Center (Narodowe Centrum Nauki) in Poland under project no. 2018/31/B/ST5/00455.

References

1 W. Li, Z. Wang, F. Deschler, S. Gao, R. H. Friend and A. K. Cheetham, *Nature Rev. Mater.*, 2017, **2**, 16099.
2 B. Saparov and D. B. Mitzi, *Chem. Rev.*, 2016, **116**, 4558–4596.
3 M. Mączka, M. Ptak, A. Gągor, D. Stefańska and A. Sieradzki, *Chem. Mater.*, 2019, **31**, 8563–8575.
4 M. Mączka, M. Ptak, A. Gągor, D. Stefańska, J. K. Zaręba and A. Sieradzki, *Chem. Mater.*, 2020, **32**, 1667–1673.
5 M. Mączka, A. Gagor, J. K. Zaręba, D. Stefanska, M. Drozd, S. Balciunas, M. Šimėnas, J. Banys and A. Sieradzki, *Chem. Mater.*, 2020, **32**, 4072–4082.
6 X. Zeng, T. Zhou, C. Leng, Z. Zang, M. Wang, W. Hu, X. Tang, S. Lu, L. Fang and M. Zhou, *J. Mater. Chem. A*, 2017, **5**, 17499–17505.
7 M. Wang, Z. Zang, B. Yang, X. Hu, K. Sun and L. Sun, *Sol. Energy Mater. Sol. Cells*, 2018, **185**, 117–123.

Open Access Article. Published on 19 May 2020. Downloaded on 2/10/2026 4:56:31 PM.
This article is licensed under a Creative Commons Attribution-NonCommercial 3.0 Unported Licence.

8 M. Wang, H. Wang, W. Li, X. Hu, K. Sun and Z. Zang, *J. Mater. Chem. A*, 2019, **7**, 26421–26428.
9 T. Zhou, M. Wang, Z. Zang and L. Fang, *Adv. Energy Mater.*, 2019, 1900664.
10 X. Zhao, J. D. A. Ng, R. H. Friend and Z.-K. Tan, *ACS Photonics*, 2018, **5**, 3866–3875.
11 W. Chen, S. Bhaumik, S. A. Veldhuis, G. Xing, Q. Xu, M. Grätzel, S. Mahaisalkar, N. Mathews and T. C. Sum, *Nature Commun*, 2017, **8**, 15198.
12 R. Shang, S. Chen, S. M. Wang and S. Gao, in *Metal-Organic Framework Materials*, ed. R. L. MacGillivray and C. M. Lukehart, John Wiley & Sons Ltd, 2014, pp. 221–238.
13 W.-J. Xu, Z.-Y. Du, W.-X. Zhang and X.-M. Chen, *CrystEngComm*, 2016, **18**, 7915–7928.
14 M. Mączka, A. Gągor, M. Ptak, W. Paraguassu, T. A. da Silva, A. Sieradzki and A. Pikul, *Chem. Mater.*, 2017, **29**, 2264–2275.
15 Y. Tian, A. Stroppa, Y. Chai, L. Yan, S. Wang, P. Barone, S. Picozzi and Y. Sun, *Sci. Rep.*, 2014, **4**, 6062.
16 L. C. Gómez-Aguirre, B. Pato-Doldán, J. Mira, S. Castro-García, M. A. Señarís-Rodríguez, M. Sánchez-Andújar, J. Singleton and V. S. Zapf, *J. Am. Chem. Soc.*, 2016, **138**, 1122–1125.
17 W.-J. Xu, P.-F. Li, Y.-Y. Tang, W.-X. Zhang, R.-G. Xiong and X.-M. Chen, *J. Am. Chem. Soc.*, 2017, **139**, 6369–6375.
18 M. Trzebiatowska, A. Gagor, L. Macalik, P. Peksa and A. Sieradzki, *Dalton Trans.*, 2019, **48**, 15830–15840.
19 Z.-Y. Du, T.-T. Xu, B. Huang, Y.-J. Su, W. Xue, C.-T. He, W.-X. Zhang and X.-M. Chen, *Angew. Chem., Int. Ed.*, 2015, **54**, 914–918.
20 M. Trzebiatowska, M. Mączka, M. Ptak, L. Giriunas, S. Balciunas, M. Simenas, D. Klose and J. Banys, *J. Phys. Chem. C*, 2019, **123**, 11840–11849.
21 F.-J. Geng, L. Zhou, P.-P. Shi, X.-L. Wang, X. Zheng, Y. Zhang, D.-W. Fu and Q. Ye, *J. Mater. Chem. C*, 2017, **5**, 1529–1536.
22 M. Mączka, M. Ptak, A. Gągor, A. Sieradzki, P. Peksa, G. Usevicius, M. Simenas, F. Furtado Leite and W. Paraguassu, *J. Mater. Chem. C*, 2019, **7**, 2408–2420.
23 M. M. Zhao, L. Zhou, P.-P. Shi, X. Zheng, X.-G. Chen, J.-X. Gao, L. He, Q. Ye, C.-M. Liu and D.-W. Fu, *Chem.–Eur. J.*, 2019, **25**, 6447–6454.
24 M. Mączka, A. Gągor, M. Ptak, D. Stefańska and A. Sieradzki, *Phys. Chem. Chem. Phys.*, 2018, **20**, 29951–29958.
25 M. Mączka, I. E. Collings, F. Furtado Leite and W. Paraguassu, *Dalton Trans.*, 2019, **48**, 9072–9078.
26 (*a*) J. M. Bermúdez-Garcia, M. Sánchez-Andújar, S. Castro-García, J. López-Beceiro, R. Artiaga and M. A. Señarís-Rodríguez, *Nature Comm*, 2017, **8**, 15715; (*b*) J. M. Bermúdez-Garcia, M. Sánchez-Andújar and M. A. Señarís-Rodríguez, *J. Phys. Chem. Lett.*, 2017, **8**, 4419–4423.
27 J. M. Bermúdez-Garcia, S. Yáñez-Vilar, A. Garcia-Fernández, M. Sánchez-Andújar, S. Castro-García, J. López-Beceiro, R. Artiaga, M. Dilshad, X. Moya and M. A. Señarís-Rodríguez, *J. Mater. Chem. C*, 2018, **6**, 9867–9874.
28 M. Mączka, A. Gągor, M. Ptak, D. Stefańska, L. Macalik, A. Pikul and A. Sieradzki, *Dalton Trans.*, 2019, **48**, 13006–13016.
29 Y. Wu, S. M. Shaker, F. Brivio, R. Murugavel, P. D. Bristowe and A. K. Cheetham, *J. Am. Chem. Soc.*, 2017, **139**, 16999–17002.
30 Y. Wu, T. Binford, J. A. Hill, S. Shaker, J. Wang and A. K. Cheetham, *Chem. Commun.*, 2018, **54**, 3751–3754.
31 Y. Wu, D. M. Halat, F. Wei, T. Binford, I. D. Seymour, M. W. Gaultois, S. Shaker, J. Wang, C. P. Grey and A. K. Cheetham, *Chem. European J.*, 2018, **44**, 11309–11313.
32 M. Ptak and M. Mączka, *Spectrochim. Acta A*, 2020, **230**, 118010.
33 H. L. B. Boström, *CrysEngComm*, 2020, **22**, 961–968.
34 S. Blundell, *Magnetism in Condensed Matter (Oxford Master Series in Condensed Matter Physics)*, Oxford University Press, New York, 2001.
35 P. G. Manning, *Can. Mineral.*, 1968, **9**, 348–357.
36 M. Li, V. Smetana, M. Wilk-Kozubek, Y. Mudryk, T. Alammar, V. K. Pecharsky and A.-V. Mudring, *Inorg. Chem.*, 2017, **56**, 11104–11112.
37 M. Mączka, D. Stefańska, J. K. Zaręba, M. Nyk and A. Sieradzki, *J. Alloys Compds.*, 2020, **821**, 153464.
38 P. Kubelka and F. Munk, *Z. Tech. Phys.*, 1931, **12**, 593–601.
39 C. Jiang, H. Fu, Y. Han, D. Li, H. Lin, B. Li, X. Meng, H. Peng and J. Chu, *Cryst. Res. Technol.*, 2019, **54**, 1800236.
40 S. Sugano, Y. Tanabe and Y. H. Kamimura, *Multiplates of Transition-Metal Ions in Crystals*, Academic, New York, 1970.
41 A. Watras, A. Matraszek, P. Godlewska, I. Szczygieł, J. Wojtkiewicz, B. Brzostowski, G. Banach, J. Hanuza and P. J. Dereń, *Phys. Chem. Chem. Phys.*, 2014, **16**, 5581–5588.
42 M. Ptak, A. Gągor, A. Sieradzki, B. Bondzior, P. Dereń, A. Ciupa, M. Trzebiatowska and M. Mączka, *Phys. Chem. Chem. Phys.*, 2017, **19**, 12156–12166.
43 S. Lin, H. Lin, C. Ma, Y. Cheng, S. Ye, F. Lin, R. Li, J. Xu and Y. Wang, *Light Sci. Appl.*, 2020, **9**, 22.

 This journal is © The Royal Society of Chemistry 2020